# Harbor Bay Business Park liquefaction during Loma Prieta earthquake - A critical state perspective

Jorge Macedo [a,*], Luis Vergaray [a], Curtis Jensen [b], Renzo Cornejo [a], Michael Jefferies [c]

[a] *Georgia Institute of Technology, Atlanta, GA, USA*
[b] *Consulting Engineer, USA*
[c] *Formerly Gulf Canada Resources, Canada*

## ABSTRACT

Part of the Harbor Bay Business Park, Alameda in California, showed evidence of liquefaction during the 1989 Loma Prieta earthquake, but this was accompanied by only small settlements and no significant damage to two recently constructed office buildings. Digital CPT records are available from a reasonably comprehensive post-earthquake investigation. These, in combination with the large body of test data associated with the Park's development, have been used to assess the soil behavior at this site further. Using analysis based on critical state soil mechanics, it appears likely that the presence of underlying Bay Mud was an important factor, with the limited undrained strength of that stratum limiting the transmitted shear stresses to the overlying and liquefiable sand fill but without preventing its liquefaction. This inferred behavior is consistent with a system (i.e., favoring interaction between layers) response, which was also observed during the 2010–2011 Canterbury earthquake sequence.

## 1. Introduction

This case history is within the Harbor Bay Isle project, which consists of 940 acres of hydraulic fill dredged from San Francisco Bay and pumped into the site after constructing perimeter dikes, starting late in 1966. Harbor Bay Isle is adjacent to the south, west, and north sides of Bay Farm Island, a district of Alameda city, California. Both Harbor Bay Isle and Bay Farm Island are separated from the rest of the city on Alameda Island by the San Leandro channel. About 600 acres were zoned as residential and the remainder as commercial; the latter is now known as the Harbor Bay Business Park (HBBP). The HBBP borders on the Oakland International Airport and the San Francisco Bay.

There were instances of liquefaction and non-liquefaction within Harbor Bay Isle during the magnitude 6.9, 1989 Loma Prieta earthquake that affected California. Liquefaction in the Harbor Bay Business Park has been referred to as Site 4 in Mitchell et al. [1] and as Alameda Bay Farm in Moss et al. [2]. However, these prior investigations used limited cone penetration test (CPT) data and also, as conventional at the time, regarded the hydraulic fill as the only soil of interest. Here we consider in more detail a 0.12 km$^2$ part of the HBBP, which was originally called Plaza 6 and then renamed the International Teleport Plaza (ITP). Our approach follows a critical state framework for both the dredged sand

fill and the underlying Bay Mud, with conventional reliance on surficial manifestations of liquefaction (there were no strong motion or piezometer records at this site).

The ITP area is enclosed by a South Loop Road and the Harbor Bay Parkway, with an aerial view and site plan shown in Fig. 1. Fig. 2 illustrates one of the two buildings constructed in the ITP before the 1989 Loma Prieta earthquake, corresponding to a standard low-rise commercial development. The extent of liquefaction shown in Fig. 1 is from an inspection of the time (Hallenbeck & Associates [3]) and the liquefaction details are discussed in the manuscript; the buildings shown on the photograph to the west and northwest of the ITP had not been constructed in 1989, and liquefaction there was a greenfield condition.

## 2. Methodology

The HBBP case history is developed using critical state soil mechanics, and it is helpful to summarize this framework as it differs from the current predominant practice. For sands, the current practice largely uses the so-called NCEER method for assessing liquefaction triggering (e. g., Youd et al. [4]) where fines content (measured or typically inferred as in the case of the Cone Penetration Test – CPT) is used in addition to penetration resistance. If sufficiently plastic, fine-grained soils are
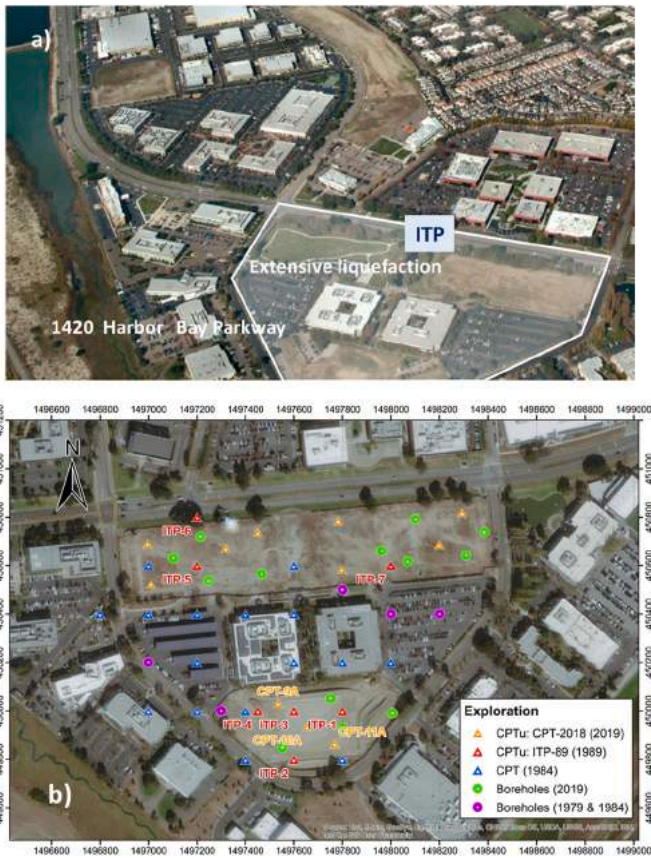
**Fig. 1.** International Telegraph Plaza layout. Representative subsurface information is shown in Fig. 3, a) Aerial view of the HBBP showing the ITP location where liquefaction occurred during the 1989 Loma Prieta earthquake, b) Plan of development from ~1985 showing site investigations and proposed buildings.



**Fig. 2.** Building at 1420 harbor Bay Parkway.

characterized as 'clay-like' and taken as non-liquefiable. In contrast, while still relying on the CPT as a key input, a critical state approach incorporates more explicitly the soil's intrinsic frictional strength and compressibility in evaluating CPT data for liquefaction assessments.

The critical state approach to soil behavior originated with the U.S. Army Corps of Engineers (USACE) nearly a century ago when constructing one of the world's first liquefaction-resistant dams at Franklin

Falls [5]. The engineering of this dam was based on the recognition that, as soil comprises particles, the distortion ("shearing") of soil generally involves a change in the void ratio (e) as the particles move past each other. If the soil is loose, the particles will tend to move to a denser state, while the opposite will occur if the soil is dense. Two particular understandings then developed: i) void ratio evolved to a unique critical-state value with distortion regardless of its initial value (Casagrande [6,7]), with this large-distortion value defining the critical state line (CSL) and being the key to understanding soil behavior as any soil that was looser would be contractive and so liquefiable if saturated (hence the name 'critical void ratio'); and, ii) soil strength developed from the combination of 'friction' (i.e., the critical state friction) and 'interlocking' (i.e., dilatancy caused by distortion) which was formalized by Refs. [8,9]. The missing idea at that time was how to link (i) and (ii); this link was provided some forty years later and was that the limiting dilatancy depended on the difference between the soil's current void ratio and its critical void ratio at the current mean effective stress, which was defined as the state parameter ($\psi$) by Been and Jefferies [10]. These three ideas are key for a modern understanding of soil behavior and apply regardless of a soil's gradation, fines content, etc. (Jefferies [11]). In particular, this framework was found necessary to understand recent liquefaction failures of three large dams: Fundão [12]; Cadia [13]; and, Brumadinho [14,15]. The critical state approach has also been found helpful in unifying cyclic liquefaction data (e.g., Refs. [16–20]).

In applying the critical state approach to the HBBP case history, the fines content's notion is replaced by the soil's stress ratio at critical state - also known as soil's intrinsic friction-i.e., $M_{tc} = q/p$, with $q$ the deviatoric stress and $p$ the mean effective stress at critical state), its compressibility ($\lambda_{10}$), and additional mechanical properties (discussed in section 4). Of note, under a critical state framework, a 'sand like' or 'clay like' separation is not required; different soils simply exhibit different mechanical properties such as $M_{tc}$, $\lambda_{10}$. Correspondingly, one of the key aspects of the case history discussed in this study becomes assessing the properties of the soils involved. A further difference to the NCEER methodology is that in a critical state approach, CPT data is not reduced to a reference stress level, but instead, the data is used as dimensionless stress-ratios in a formal inversion following the laws of mechanics (the inversion process is discussed in section 5). Thus, the final output is the site response being characterized in terms of the in-situ state parameter, which is linked with mechanical soil properties. These aspects are illustrated later in the manuscript.

## 3. Ground conditions

### 3.1. Regional setting

The field investigations at the ITP site extended through an existing Fill, the Holocene Bay Mud sediments (HBM, often just called 'Bay Mud' in the documents of the time), the Merritt Sand, and at some instances into the Pleistocene Bay Mud (PBM) sediments, also known locally as the Old Bay Clay or just the Old Bay Mud. These formations are described in detail in the subsequent sections.

This sequence is underlain by the Alameda formation and then a dense Jurassic-Cretaceous bedrock of the Franciscan formation bedrock; none of these strata were investigated at the ITP. Rogers and Figuers [21] summarized data from some 200 deep borings in the greater Oakland area, reporting a bedrock depression beneath Bay Farm Island and Oakland International Airport with bedrock at a depth of about 300 m.

### 3.2. Site investigations

Initial geotechnical investigations of the HBBP began about 1979 and included mechanical CPT's and rotary test borings. As the site developed, further site investigations were carried out with the electronic CPT used from the early 1980s for which digital records exist. As can be seen

in Fig. 1, the investigations amount to a grid of CPTs supplemented by sampled borings (also illustrated in Fig. 1). Additional CPT data to ITP is available from other investigations nearby, including digital data for pre-earthquake conditions.

Seven CPTu's were performed in the Fall of 1989 on sites where liquefaction was observed, with the location of seven of these being shown in Fig. 1 (denoted as ITP N°1, etc.); these were modern CPTs with the standard pore pressure sensor location (i.e., the $u_2$ location). This data is in digital form and is processed here using modern methods for evaluating ground conditions from the CPT. These CPT soundings were supplemented by a further twelve CPT soundings carried out in three campaigns of four soundings, each that were separated by several weeks to evaluate post-EQ aging effects. Shear wave velocities were also measured at the site. CPT soundings have continued since 1990 as the HBBP has been developed. For instance, CPT soundings were made in the ITP in 2018 for a new development (Langan [22]), with some of these to a depth of about 25 m below ground surface, deeper than what was attained by the immediate post-earthquake CPTs of 1989. The extensive CPT soundings (Langan [22]) have been complemented by sampled borings, with some eighteen borings put down at the site to define the fill and underlying natural ground; these borings extended to the base of the Bay Mud.

Laboratory testing was limited to index and gradation during the development of the HBBP (1980–2018). In 2020, a bulk sample of the hydraulic fill was recovered from the ground surface in an area that had been exposed by construction activities. The sampling location was slightly more than 30 m north of 1420 Harbor Bay Parkway (one of the two buildings that were on the ITP before the Loma Prieta earthquake) within a current building construction site. This bulk sample has been used for measuring the mechanical properties of the hydraulically placed sands, as discussed later.

### 3.3. Stratigraphy

The first soil layers at the ITP consist of a hydraulic fill, which was ubiquitously dense to very dense near the surface, grading from loose to very loose at depth. The fill overlies natural soil, with the top of the HBM layer defining the transition between fill and natural soil. The HBM is underlain by Merritt Sand, underlain in turn by soils of the PBM sequence. The water table lies about 1.5–2.5 m below the ground surface, which is slightly above mean sea level. The CPT data indicates hydrostatic conditions in the sands at the site. Fig. 3 shows the typical ground conditions encountered within the HBBP to up to 25 m depth. Stratigraphic boundaries have been picked using the combination of CPT resistance (e.g., the tip resistance, $q_c$), the normalized measured excess pore pressure ($B_q$), and friction ratio ($F$), which is a standard approach. The typical stratigraphic sequence at the ITP is illustrated in Fig. 3. This sequence is also consistent with the stratigraphy at the Naval Air Station (USGS [23]), which is at an approximated distance of 7 km and it is the site of the nearest strong-motion station. Nine soil zones are recognized within the upper 25 m of the ITP. Some stratigraphic boundaries are sharp, for example, that of the HBM to Merritt Sand, while those within the PBM are more gradational. Some variation in soil behavior occurs within each identified stratum, which is usual. The stratigraphic units are now discussed in turn using the typical profile in Fig. 3.

Layers 1 and 2 are hydraulic fill, with Layer 1 being sufficiently above the groundwater such that construction equipment could move on it (possibly densifying it) while Layer 2 reflects the hydraulic fill in its as-placed condition. The deeper parts of the hydraulic fill were interbedded with soft clay trapped in the fill during filling and referred to as "slurry" in logs and documents of the time. Numerous samples were tested for their water contents. Samples with water contents of about 20% are likely silty sands broadly similar to the gradation envelope for the fill: Layer 3. Water contents in the 30%–40% range probably included sand/
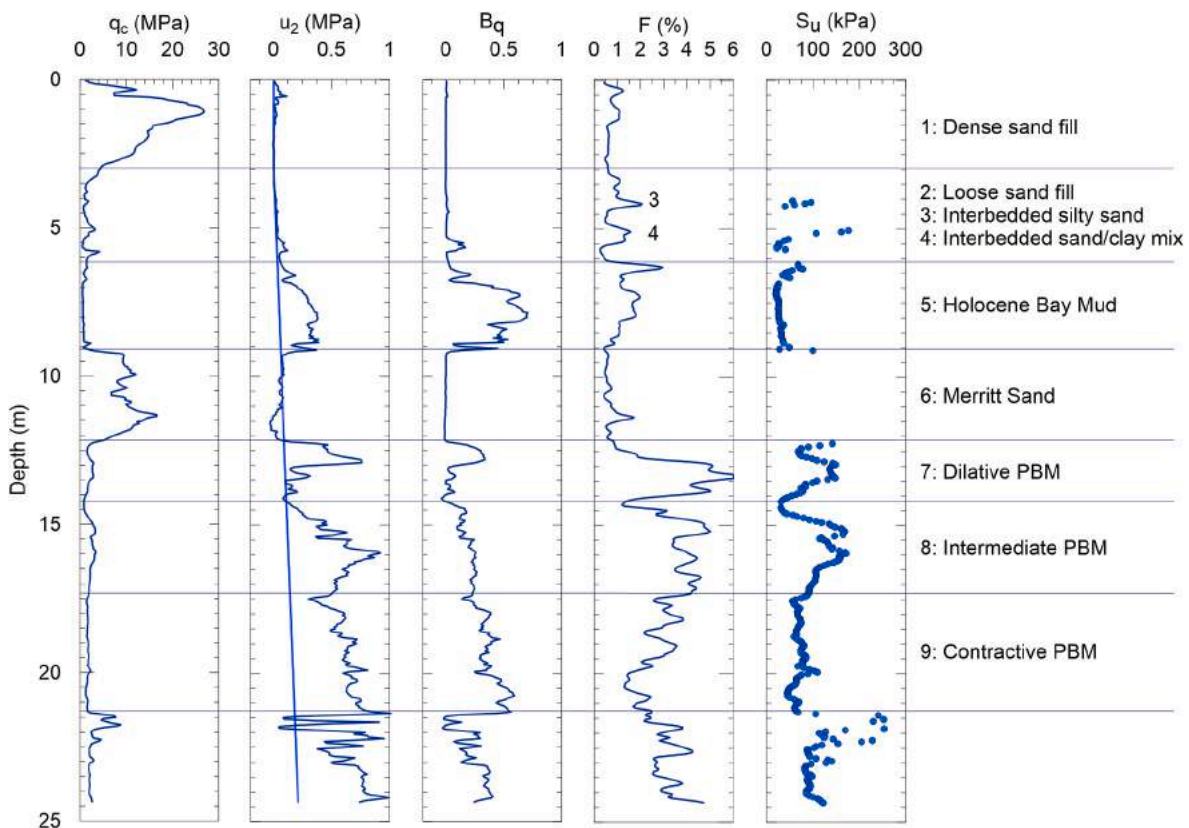


**Fig. 3.** Stratigraphy at HBBP from a deep CPT record (data courtesy of Langan).

clay mixtures, the clay being plastic: Layer 4. There were a few water contents of 50% and above in layers logged mainly as sandy, but these are believed to be isolated pockets. The boring logs also indicate that the soft, plastic clay "slurry" was also encountered as thin seams as well as thicker layers.

The boundary between the fill (about 20 years old in 1989) and the underlying natural soils is the top of Layer 5, the Holocene Bay Mud. The HBM was encountered in most of the borings, except for those near Harbor Bay Parkway. The transition elevation did not vary much, ranging from about 26.2 to 27.1 m and averaging 26.7 m with a standard deviation of 0.4 m. This stratum thickens, but not smoothly, from northwest to southeast across the ITP.

The top of layer 6 is the transition to much older soils and soils found elsewhere in the region. Layer 6 is a silty sand, called Merritt Sand by other workers (e.g., USGS [23]). It was encountered in all CPTs. The top of layer 7 is the start of the PBM sequence. There are multiple sub-units within the underlying Pleistocene Bay Mud identified as Layers 7, 8, and 9. These layers comprise clay and silt strata to a considerable depth; the full depth of this unit was not identified in the HBBP, but it has a thickness of some 40 m at the Naval Air Station.

## 4. Soil properties

### 4.1. Sand fill (layers 1 and 2)

The hydraulically placed sand fill has a median grain size range of $160 < D_{50} < 220$ μm and a fines content of less than 20% (typically about 10%), illustrated in Fig. 4. A sample of this fill collected in 2018 was used for triaxial testing to determine the mechanical properties, following the protocols given in Jefferies & Been [24]. The CSL determined is shown in Fig. 5.

The triaxial testing on HBBP fill was supplemented using data on similar sands, in particular, to quantify the effect of changing fines content on the fill mechanical behavior. A large body of fill testing was carried out for oil exploration in the U.S and Canadian arctic offshore, deriving on data on the public domain (Jefferies and Been [25]). This data was searched, and Isserk sand, a predominantly quartzitic sand with no plastic fines as the collected fill, was identified as gradationally similar to the HBBP fills (see Fig. 4). Interestingly, the CSL of Isserk sand with 5% fine contents (indicated as Isserk 220/5 in Fig. 5) is also consistent with that of the collected fill (see Fig. 5), which also has similar fine contents. The tests on Isserk sand with 5% and 10% fine contents are used in this study to include gradational effects on assessing the in-situ state of the fill sands. For instance, the CSLs of the two Isserk sand gradations are shown in Fig. 5 to illustrate the effect of changing fines; increasing fines increases the slope of the CSL ($\lambda_{10}$), a behavior
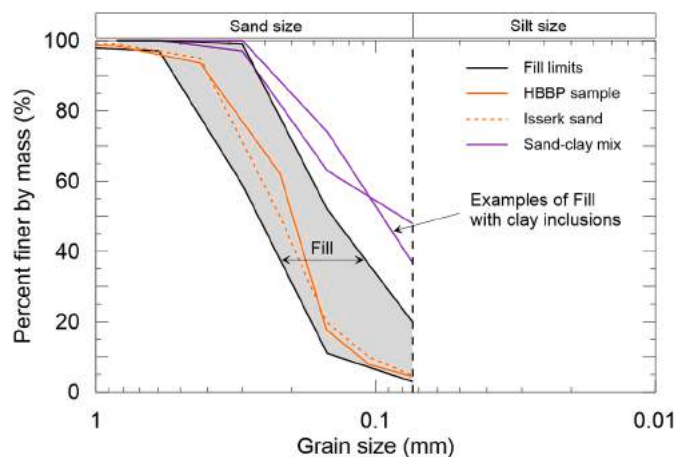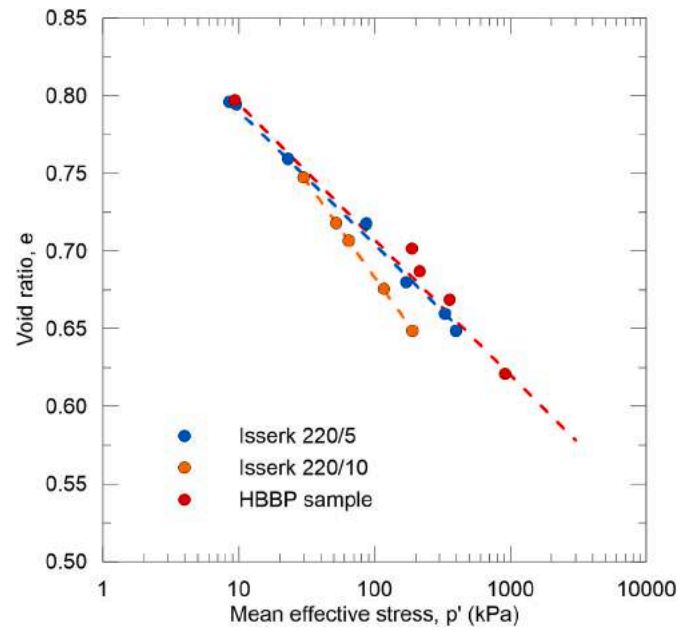


**Fig. 5.** Critical state locus of the HBBP fill sand and the Isserk sands with gradations of 5% and 10%.

encountered with other sands (Jefferies and Been [25]). This feature will be used subsequently on identifying the in-situ state of the fill sands (see section 5).

The corresponding strength data representative of the fill materials is shown in Fig. 6, with the strength properties $M_{tc}$ (already defined) and $N$, which is the volumetric coupling in a strength-dilatancy relationship $(q/p)_{max} = M_{tc} - (1 - N) D_{min}$, where $D_{min}$ is the maximum dilatancy. The effect of soil state on the limiting ("peak") dilation rate is shown in Fig. 7 through the state-dilatancy parameter $X$, which represents the scaling of $D_{min}$ and the soil state, using the state parameter ($\psi$) as defined in Been and Jefferies [10]. $M_{tc}$, $N$, and $X$ can be calculated from triaxial tests with procedures detailed in Jefferies and Been [25], which we have
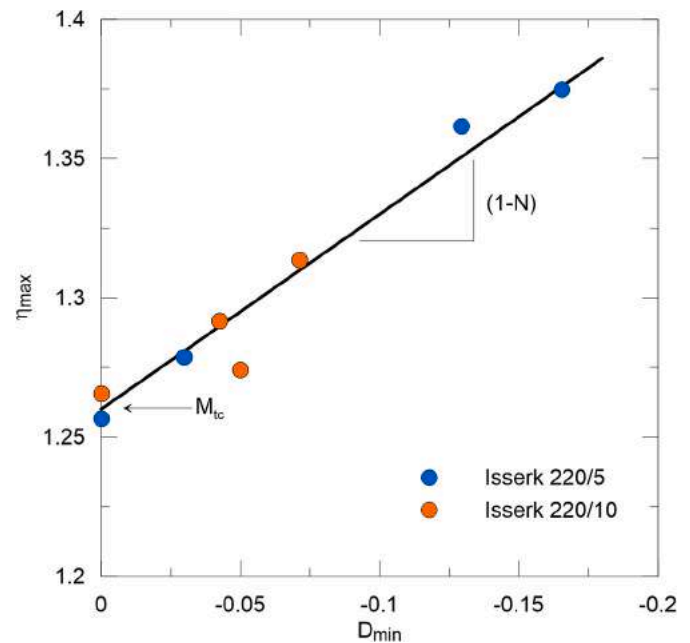


**Fig. 6.** Effect of the maximum dilatancy ($D_{min}$) on the drained strength of the sand fill. $\eta_{max}$ corresponds to the maximum $\eta$ during each test, and $M_{tc}$ is the stress ratio at the critical state.
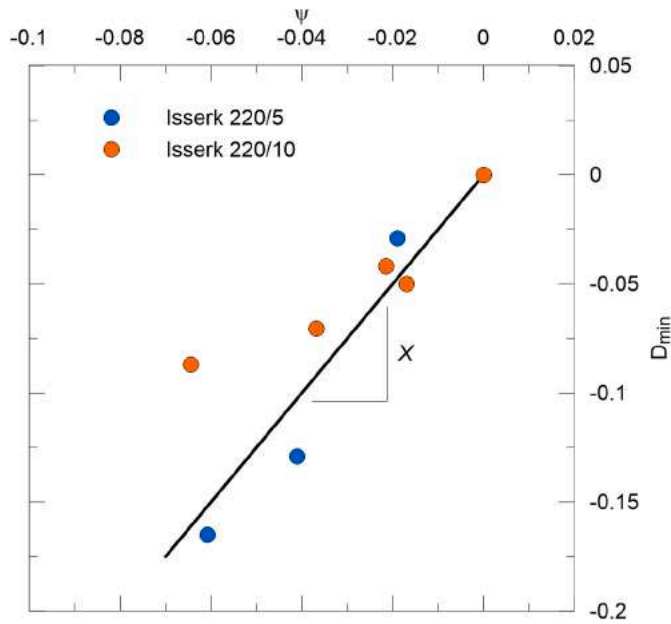


**Fig. 4.** Gradation envelope of HBBP fill, recovered HBBP sand, Isserk sand, and examples of fill with slurry inclusion.

**Fig. 7.** Control of maximum dilatancy ($D_{min}$) by state parameter ($\psi$).

followed in this study. Sand properties are summarized in Table 1, with the meaning of the properties annotated on the respective figures.

### 4.2. Compromised fill (Interbedded layers 3 and 4)

Layers 3 and 4 appear as intermingled soils within the extensive Layer 2, with questionable lateral continuity. There are no triaxial tests or similar on either 3 or 4 layers, so the properties must be estimated. In the case of Unit 3, its compressibility is assessed (see section 5) from the CPT data based on its 'soil behavior type'. Unit 3 appears to retain the characteristics of the parent sand fill but with increased compressibility caused by the included mud. In the case of Unit 4, it appears to be disturbed/remolded Bay Mud; its properties have been taken as the weak end of the spectrum of Layer 5 discussed subsequently.

### 4.3. Bay Mud (Layer 5)

Undisturbed samples of the Holocene Bay Mud were tested in the laboratory. Both compressibility (oedometer) and the undrained strength (undrained triaxial tests) were measured. These undisturbed samples showed high water contents, presented as a void ratio versus the in-situ vertical effective stress of the sample ($\sigma'_{v0}$) on Fig. 8 below; void ratios were commonly greater than 2. The CSL and $\psi$ contours are approximated to match the observations in Figs. 18 and 19 (discussed later) and are shown only for illustrative purposes (see Fig. 8's caption).

The sand fill had been in place for at least 15 years when the first oedometer samples were taken, and full dissipation of fill-induced excess pore pressure should have occurred within about six years based on the measured coefficients of consolidation ($c_v$).

The HBM surface elevation indicates that the HBM was always submerged by the Bay as the surface was below mean low water elevation with desiccation unlikely. Thus, no apparent over-consolidation from aging or other geological processes would be expected. Other workers

**Table 1**
Summary of fill properties.

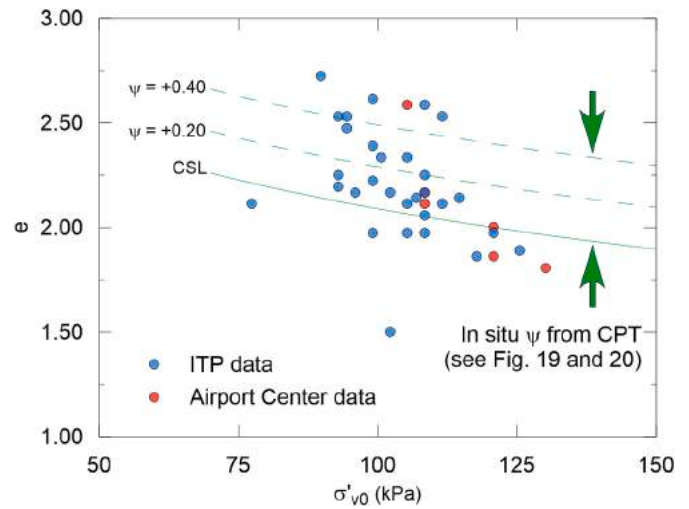| Soil | $D_{50}$ (μm) | Fines | $\lambda_{10}$ | $M_{tc}$ | $N$ | $X$ |
|---|---|---|---|---|---|---|
| HBBP (2020) | 220 | 5% | 0.09 | 1.24 | – | – |
| Isserk 220/5 | 220 | 5% | 0.086 | 1.26 | 0.3 | 2.7 |
| Isserk 220/10 | 220 | 10% | 0.123 | 1.26 | 0.3 | 2.7 |



**Fig. 8.** Insitu void ratio of Holocene Bay Mud. The CSL and $\psi$ contours are approximated to match the observations in Figs. 18 and 19 and are shown only for illustrative purposes. The CSL is estimated by recovering a $\psi = -0.05$ (Fig. 19) for an initial void ratio of 2.04 at a mean pressure of 100 kPa (Fig. 18).

have found similar normally consolidated conditions in the HBM elsewhere (e.g., Refs. [26–28]). These conditions are reflected in the void ratios of the in-situ HBM samples being predominantly looser (wetter) than the estimated critical state locus (see below), as shown in Fig. 8. The initial compression index ($C_c$) was largely in the range $1.05 < C_c < 1.37$ with a representative $C_c \sim 1.10$. However, most unusually, the swelling (elastic) index was small with a consistent $C_s/C_c \sim 0.1$; this is about half the elastic void ratio recovery normally expected for soft clay.

The strength tests were only performed on samples that did not display visible signs of disturbance. Strength was taken as the peak of the stress-strain curve or the stress at 10% strain, whichever occurred first. The data is shown in Fig. 9, normalized by the in-situ vertical effective stress ($\sigma'_{v0}$); the undrained strength ratio lies in the range $0.2 < s_u/\sigma'_{v0} < 0.4$, a usual range for normally consolidated clay. The undrained strength ratio was also computed from the CPT using the cone factor $N_{kt} = 16$ (a value routinely used for HBM); this data also being shown in Fig. 9 but now plotted against the normalized excess pore pressure coefficient $B_q$ since void ratio was unknown at each CPT data scan. The range and mean strength ratio of strengths from the two CPT soundings, ITP-3 and ITP-4, was similar to strengths measured with laboratory samples and largely also unaffected by $B_q$ similar to the lack of effect of void ratio seen in the compression test. Conversely, the other two CPT soundings, ITP-1 and ITP-2, while exhibiting similar strength ratios to the laboratory compression tests for $B_q > 0.7$ (= truly normally consolidated as conventionally understood), show a more usual trend of improving strength with decreasing $B_q$ (i.e., an apparent effect of in situ state).

The undrained strength of soils scales with $M_{tc}$. Meehan et al. [29] carried out drained direct shear tests on remolded Bay Mud and obtained large-deformation values in the range 23.3 deg $< \varphi_{cv} <$ 25.2 deg; taking an average of this range, this is equivalent to $M_{tc} \sim 0.95$. Sitar and Salgado [26] reported on the response of the Buy Mud in cyclic simple shear, their data being presented after normalization by the static undrained strength. A reasonable average strength is $s_u/\sigma'_{v0} \sim 0.3$ from the laboratory tests shown in Fig. 9a, which then gives a cyclic strength trend from the Sitar and Salgado [26] data, as shown in Fig. 10. This figure also shows several other examples for silts, and the trend for Bay Mud is not exceptional.
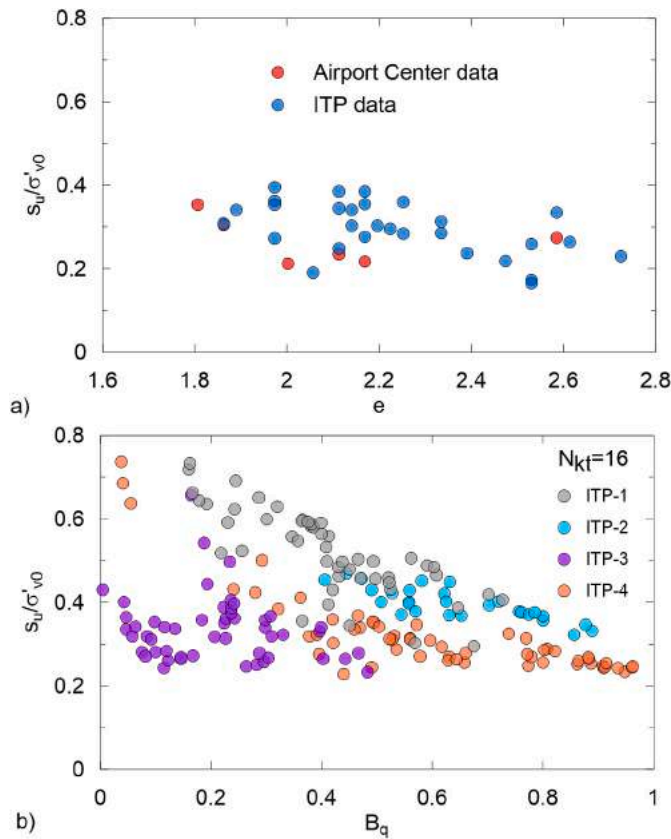
**Fig. 9.** Undrained strength ratio of Holocene Bay Mud, a) Undrained strength of undisturbed samples from laboratory tests, b) undrained strength from CPT.
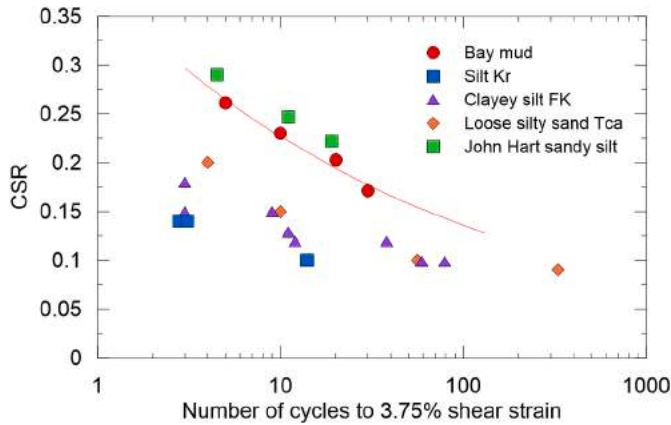


**Fig. 10.** Cyclic strength of Bay Mud in cyclic simple shear tests compared to other silts.

## 5. Soil state

### 5.1. Overview of CPT processing

Soil state (density, over-consolidation, state parameter) is primarily assessed from CPT data. The CPT measures a mechanical response that depends on both the soil's properties (e.g., compressibility as identified by Campanella et al. [30]) and the in situ state parameter so that assessing the soil state from the CPT should account for the soil's properties – a soil-specific calibration is needed. However, soil properties can vary somewhat within a stratum and certainly between strata. If a stratum can be simply identified; for instance, the HBM unit is clear in

Fig. 3, a representative calibration can be assigned for that formation based on the measured or estimated soil properties. This calibration can be computed for both drained and undrained penetration, for example, using scaled cavity expansion theory (Shuttle and Jefferies [31]). If the stratum contains either a mix of soils or is a transitional boundary between strata, then the effect of changing properties should be part of the data processing; this is done using the notion that the CPT senses 'soil type' (the familiar idea of soil classification charts for the CPT, Fig. 12 being an example of this) and soil types have 'representative' properties. Thus, the data processing can be automated to capture the effect of changing soil type using the time-synchronized CPT measurements, i.e., tip resistance ($q_c$), sleeve friction ($f_s$), and pore pressures ($u_2$) triplets ("scans," which are commonly at 20 mm intervals). The first step in doing this was the 'Plewes Method' (Plewes et al. [32]) which went even further and unified both drained and undrained calibration by assuming that including the measured $u_2$ in the data processing was sufficient to capture the difference between drained and undrained conditions.

The Plewes Method is widely used in practice, even in such significant engineering as understanding the Brumadinho dam failure by static liquefaction (Robertson et al. [14]). But, the Plewes Method was developed using the limited data on soil response to the CPT available in the early 1980s and has never been updated. Recent data suggests that the embedded relation between the normalized CPT friction ratio ($F$) and the CPT-based soil classification index remains valid on average but with quite substantial soil to soil variability (Reid [33]). It is also now known that there is a clear step-change in calibration at the drained to undrained transition, which occurs at about *IcBJ* (the soil classification index defined in Been and Jefferies [34]) ~ 2.3. The CPT processing used here involves a modified Plewes Method for the sand fill units, where penetration is drained with the range in gradation influencing the CPT calibration; the modification is described in the next sections. The HBM unit is processed using a single soil-specific calibration, as also discussed later. The Merritt sand and deeper strata are assessed in a screening-level assessment from available CPTs.

### 5.2. Comparison of CPT before and after the 1989 Loma Prieta earthquake

Automated procedures like the Plewes Method require time-coherent data, effectively only being usable with digital records. But, such digital recording did not become standard until the late 1980s. Thus, a detailed evaluation of this site depends on post-earthquake measurements from 1989 rather than the pre-earthquake 1984 CPT that only had paper records – and which leads to the question: did the earthquake affect the CPT data? This question is considered first before characterizing the strata identified in Fig. 3.

There are locations where CPTs were carried out during 1984, at which time the fill was about ten years old, and where CPTs were pushed at a nearby location after the earthquake. Example comparisons are presented in Fig. 11, the comparisons being made by scanning the 1984 paper records and then overlaying the 1989 data. The pale grey lines on Fig. 11 are 1984 data, the dark lines the matching 1989 post-earthquake pair.

The middle-overlay of Fig. 11, the ITP-5 pair, exhibits a few depth misalignments, but that is normal for CPT soundings even as close as a few meters. The $q_c$ values of the loose sand fill and underlying HBM are similar between 1984 and 1989 with possibly a small reduction of tip resistance in the loose sand; thus, a small effect of the earthquake on CPT resistance at this location within the precision of the 1984 record is a possible slight reduction of tip resistance.

In the left-hand overlay of Fig. 11, the ITP-2 pair, the zone annotated as *A* has much less resistance post-earthquake; plausibly, this could be where there was an upward movement of sand after liquefaction ('ejecta'). Apart from this loosened zone, the remainder of the profile is consistent with the 1989 data being an adequate representation of the site prior to the earthquake.
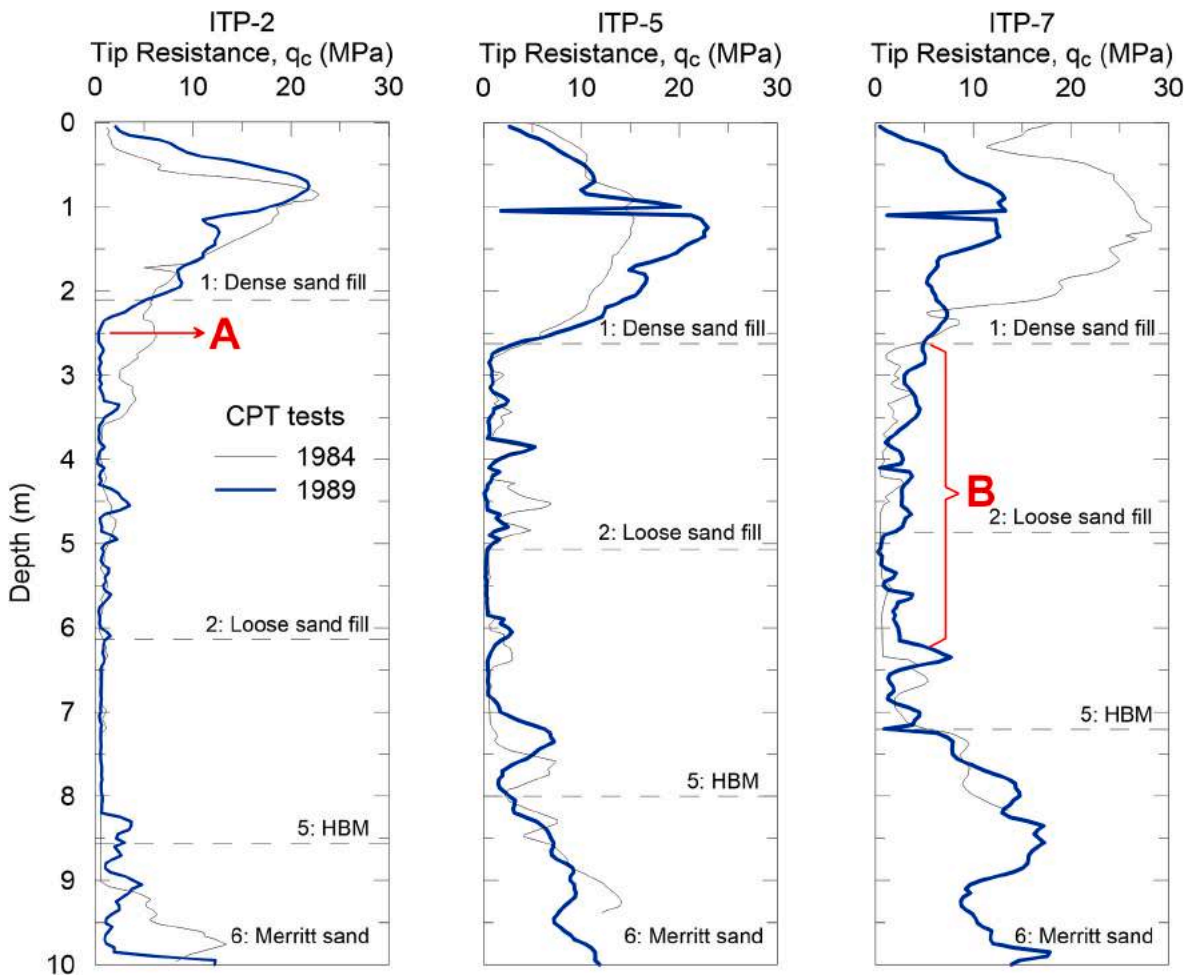
**Fig. 11.** Comparison of paired CPT resistance profiles before and after the Loma Prieta earthquake.
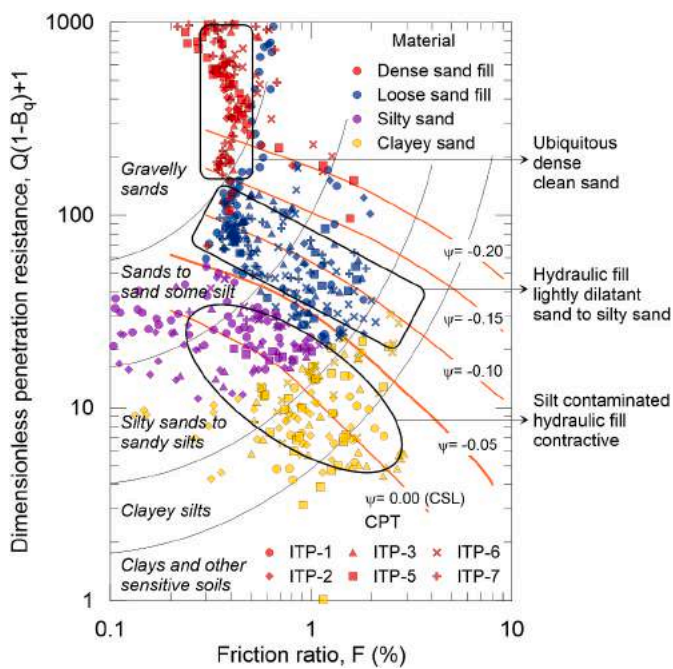


**Fig. 12.** CPT data within the hydraulic fill as a soil behavior type.

The last overlay of Fig. 11, the ITP-7 pair, gives an opposite view with clear densification of the zone annotated as *B*.

It is standard to use post-earthquake measurements as indicative of the prior conditions (e.g., Mitchell et al. [35]), and that is forced for detailed analysis of this case history because only CPT campaigns later than 1989 had the needed digital data acquisition. The comparison of this digital data with the older paper records suggests that, on average, this is acceptable but that the 1989 records will have greater dispersion of the tip resistance within the loose sand fill. As far as can be judged, because of the limited available resolution of the 1984 data, the HBM shows a similar response in 1989 as 1984.

### 5.3. Hydraulic sand fill

The results of the 1989 CPT soundings within the sand fill, layers 1 and 2 on Fig. 3, are shown in the Jefferies and Been [24] 'soil behavior type' chart in Fig. 12. This chart also shows "screening" level contours of $\psi$, which are useful for an initial appreciation. The upper 2 m or so, Layer 1, is the 'ubiquitous dense' stratum across the site and is very dilatant ($\psi < -0.2$) and presents as clean sand. In parts, this layer is very dense. It is above the water table, and thus its only role in the lique-faction is as an overlying stiff mass. The underlying sand fill, Layer 2, plots as rather heterogeneous with soil type ranging from 'sand, some silt' through to 'silty sand'; exactly as expected from the gradations determined on the fill samples. The data tends to follow a constant-state contour ($\psi \approx -0.1$), an aspect of soil development/accretion that has been found elsewhere (Reid and Jefferies [36]); in essence, the soil naturally compensates for the changes in gradation from place to place

within a similar depositional environment giving similar mechanical behavior despite the changes in gradation.

The silt and clay inclusions of Layers 3 and 4 show no systematic trend to parallel a constant-state contour; at this level of data compilation, these layers show an almost random range of gradations and an equally random range of state: from slightly contractive to very contractive. Based on the understanding of Layers 3 and 4 from the borehole records, these two layers were distinguished using the measured $B_q$: $B_q > 0.05$ was taken as Layer 4. If not Layer 4, the fill was processed using a drained inversion with the inversion coefficients depending on $F$ as detailed in the following.

The in-situ $\psi$ depends on the stress-normalized CPT tip resistance $Q$ through:

$$m\,\psi = -\ln(Q\,/\,k) \qquad [1]$$

where $k$, $m$ are the soil-property-dependent inversion coefficients. These coefficients were computed using Norsand (Jefferies [37]) in cavity expansion, scaling to the worldwide database of CPT calibration chamber studies (Ghafghazi and Shuttle [38]). The properties used are those given in Table 1, with an example of the numerical results being shown in Fig. 13 for the 10% fines sand. There is a small effect of the elastic rigidity ($I_r$) on the CPT resistance, but this has been neglected by using an average trend because it is second-order to the more important effect of changing gradation.

The CPT data plotted in Fig. 12 suggests that the least-fines fill, with about 5% fine contents (Fig. 4), can be associated with $F \sim 0.3\%$. The average fines content of the clean fill is 10%, and there is a clear concentration of data at $F \sim 0.4\%$. The computed $k$ for the properties given in Table 1 have been associated with these respective values and plotted in Fig. 14; the Plewes Method trend for an average sand with $M_{tc} = 1.25$ is also shown in this figure. The ITP-specific calibration for both 5% and 10% fines is weaker (i.e., lower $k$) than the backbone-trend in Plewes Method; the dashed line shows the modification to the Plewes Method to account for site-specific calibration.

The second inversion coefficient ($m = 5.5$) was similar for both the 5% and 10% fines fill. An average value was used regardless of the CPT friction ratio. The drained-undrained transition was established by plotting the measured $B_q$ versus the soil type index ($IcBJ$), Fig. 15. There is a near "wall" at $IcBJ \sim 2.3$ for this site (see Fig. 15). Accordingly, the data processing to infer state within the fill considers $k$ from Fig. 14 and $m = 5.5$ for $IcBJ < 2.3$.

The results of processing the CPT data within the sand fill (i.e., the soils lying above the top surface of the HBM) are shown in Fig. 16. Aside from the very dense sand ($\psi < -0.2$), the fill presents systematically looser than inferred by the 'screening level' guidance contours on
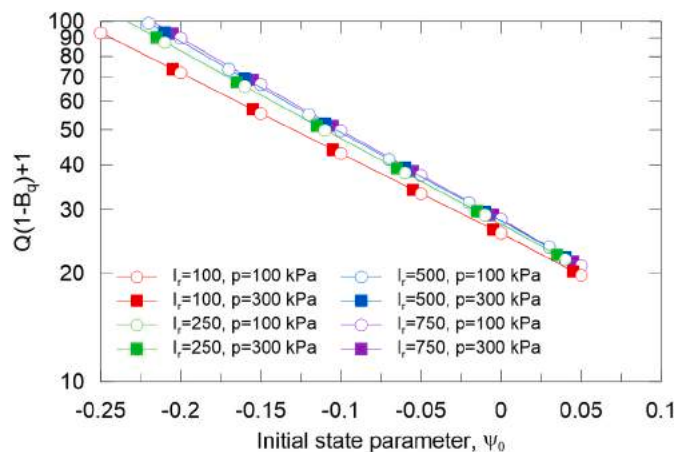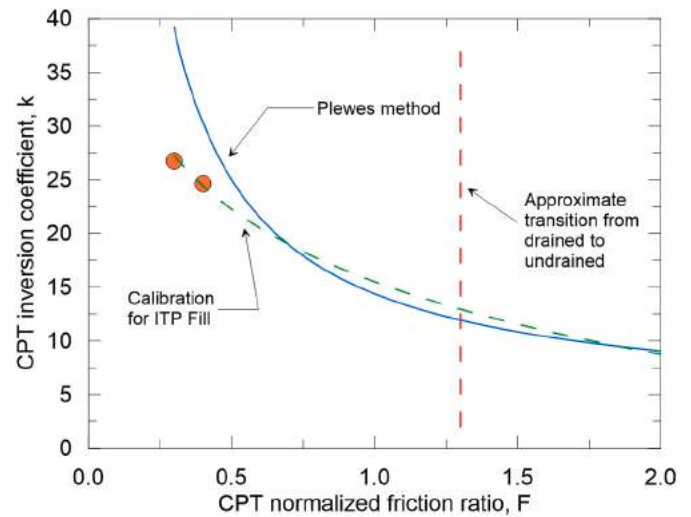


**Fig. 14.** ITP-specific calibration for inversion coefficient $k$ in sand fill.
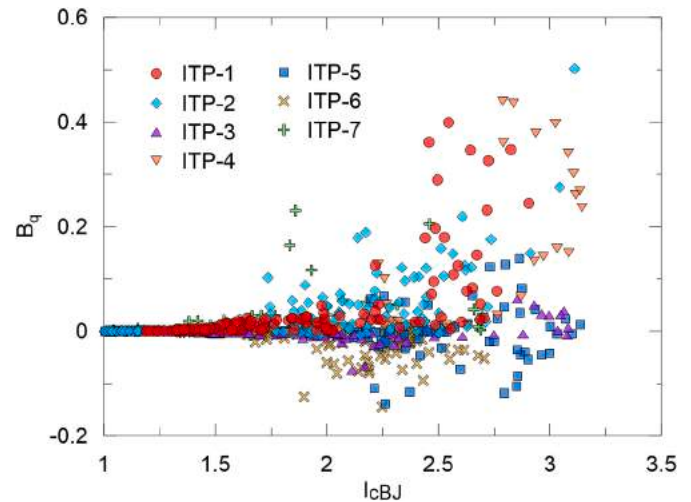


**Fig. 15.** Drained-undrained transition in CPT soundings at ITP.

Fig. 12, with the calibrated procedure, indicating $-0.05 < \psi < +0.2$ for most of the data. In terms of liquefaction, the loose fill is obviously a contributor to the site behavior during the Loma Prieta earthquake.

### 5.4. Holocene Bay Mud

The south side of the ITP is underlain HBM, and the results of the 1989 CPT soundings within the Bay Mud are shown in Fig. 17. This stratum plots as a brittle, sensitive silt, rather different from the perception of a plastic normally consolidated soft clay. There are sandy stringers within the HBM, which present as loose, but that is most likely an artifact of having soft silt above and below (no 'thin layer' correction has been used).

The NorSand implementation of critical state theory was calibrated to the Bay Mud, the calibration being shown to monotonic simple shear data reported by Rau and Sitar [27]) in Fig. 18. Test MONO-8 was chosen as that was one of the loosest tested with a void ratio $e = 2.04$ at an effective vertical stress of 100 kPa, a void ratio and stress combination that is within the range of the in situ conditions at the site albeit at the denser end of the range. The calibration adopted $\lambda_{10} = C_c$ (not unreasonable for a fine-grained material and $C_c$ having been measured, as discussed earlier), $C_s/C_c = 0.1$ (characteristic of measured values), $M_{tc} = 0.95$ (measured, discussed earlier), $N = 0$ (a 'not unreasonable'
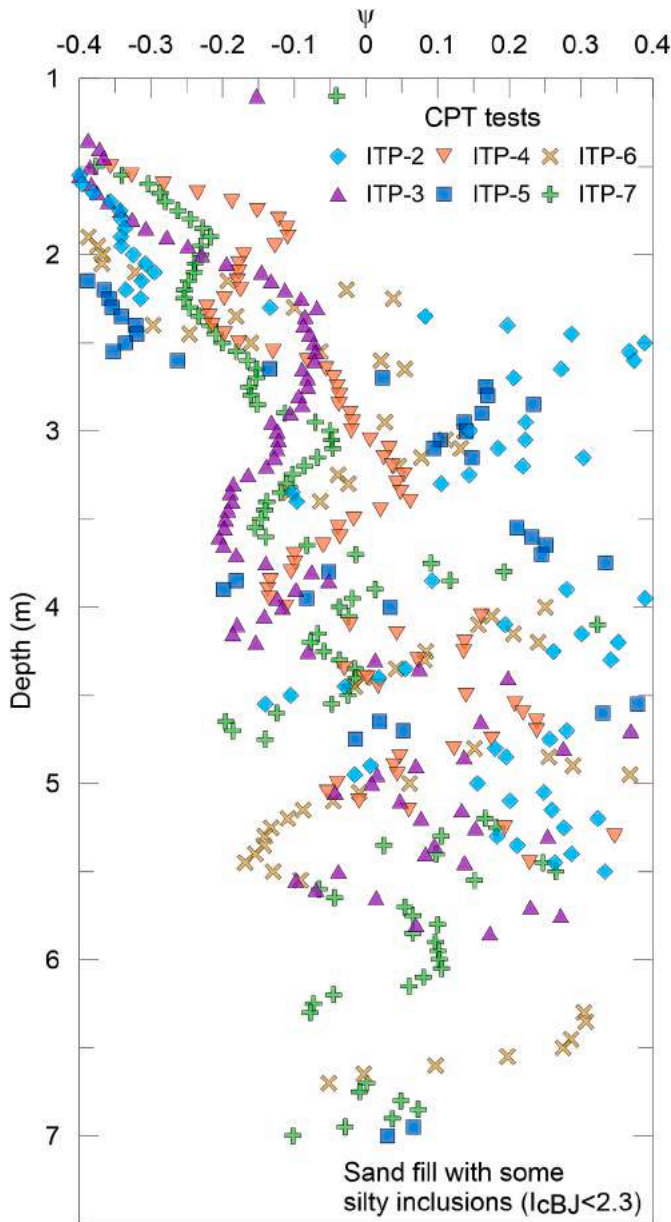


**Fig. 13.** Example of computed CPT inversion considering various elastic rigidity ($I_r$) and initial mean pressure ($p$) values.

**Fig. 16.** Inverted $\psi$ below water table within the fill at ITP from 1989 CPT soundings.



**Fig. 17.** CPT data within the Holocene Bay Mud as soil behavior type.



**Fig. 18.** Calibration of NorSand (red) to Bay Mud Test MONO- 8 (blue) in monotonic simple shear tests. The MONO tests come from Rau and Sitar [27].

value for silts) and over-consolidation ratio $OCR = 1$ (as reported by Rau and Sitar [27]). Other properties, and the state parameter, were then iterated to get a representative fit of the measured stress-strain curves; the achieved fit was for a lightly dilatant state $\psi = -0.05$, a state-dilatancy coefficient $X = 2$, and a plastic hardening modulus $H = 6$.

The calibrated soil properties were then carried forward into the inversion of the CPT data to compute the in situ state. The methodology uses the measured CPT data, which is normalized using the excess pore pressure at the $u_2$ location:

$$m'\psi = -\ln(\overline{Q}/k') \qquad [2]$$

where

$$\overline{Q} = Q(1 - B_q) + 1 \qquad [3]$$

and $k'$, $m'$ are the soil-property-dependent inversion coefficients. These coefficients were computed using the cavity inversion in Shuttle and
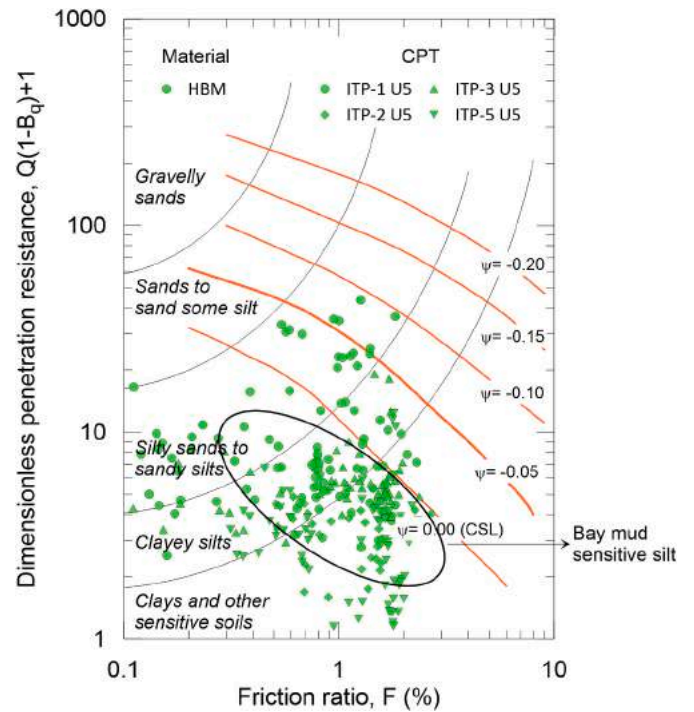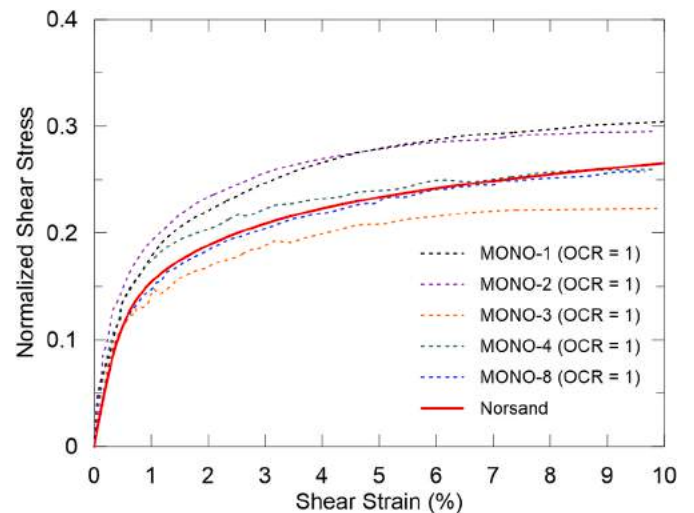
Jefferies [31], with an updated version of the software for direct use with $u_2$ data; this update was validated in the Cadia silt (see Figure E4-5 of Morgenstern et al. [13]). The computed inversion coefficients, using the HBM properties as per Fig. 18, were $k' = 6.5$, $m' = 2.6$, and the results of processing the CPT data with these coefficients are shown in Fig. 19.

A first point to note in Fig. 19 is the state used to calibrate test DSS-MONO8 (Fig. 18), which is well-aligned with the denser computed in-situ state and consistent with that test being at the low end of the in-situ void ratios. The in-situ state range computed from the CPT is also consistent with the data in Fig. 8. Going further, the "classical geological" idealization of 'normal consolidation' is for the NCL to parallel the CSL in $e - log(p')$ space with an offset of about a factor of 2 measured on the $p$-axis; if this is converted to void-ratio, 'normal consolidation' amounts to $\psi \sim 0.8/(\lambda - \kappa)$, where $\lambda$ is the CSL slope in natural log units
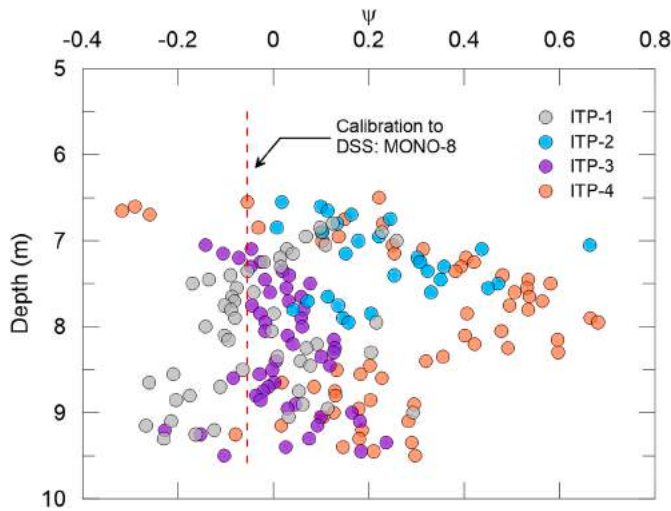
**Fig. 19.** Computed in-situ state of Bay Mud.

and $\kappa$ the swelling index, or $\psi \sim +0.3$ in the case of the Bay Mud. As can be seen in Fig. 19, the computed in-situ state from the CPT inversion is generally a little denser than $\psi = 0.3$, consistent with the Bay Mud being normally consolidated but then experiencing secondary consolidation (aging). Thus, what is computed for the in-situ state is consistent with the current understanding of the Bay Mud "in general." But, where the HBM at this site departs from accepted understanding is a layer between 7 m and 8 m depth present at ITP-2 and ITP-4 where the HBM is markedly looser with $\psi > +0.4$; at the simplest level, this assessed looseness is also evident from the CPT data as $B_q > 0.6$ in these soundings (Fig. 9b).

The effect of this range of in-situ states on undrained strengths is shown in Fig. 20, computed using the soil's properties as discussed above. The strengths at 15% strain are consistent with the undrained strength data shown in Fig. 9, with the range in measured strengths simply reflecting the range of state of the tested samples. The very weak strength computed, and not seen in the test data, is likely because such samples would have been classified as "disturbed" and thus not tested.

Although the Bay Mud presents on the 'soil behavior type' chart as predominantly sensitive clayey silt, the computed stress-strain behavior of the very loosest parts of the Bay Mud is simply just weak with minimal post-peak strength loss (Fig. 20). This computed response is a consequence of the soil's extraordinarily large compressibility.
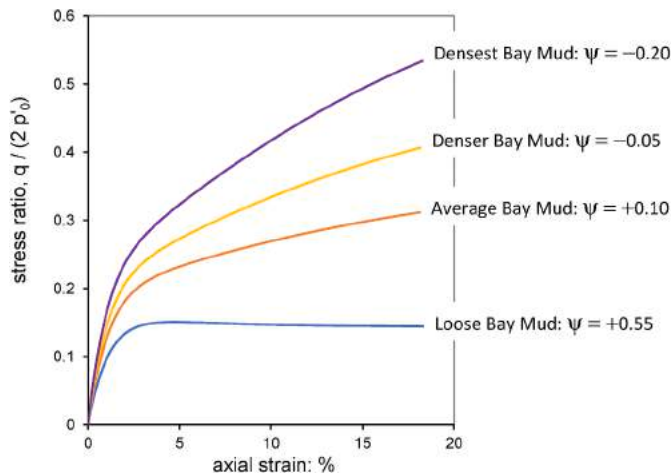
### 5.5. Older sediments

Data for the older sediments come from more recent (2018) CPT soundings in an adjacent area of the HBBP, where three soundings were pushed to some 25 m depth. The results are shown as soil behavior type in Fig. 21.

The Merritt Sand presents as dense sand, some silt grading to silty sand in parts. The soundings in this unit showed negative excess pore pressure (see Fig. 3), indicating at least only partial drainage; this suggests this unit is gradationally finer than indicated by its soil behavior type. The density of these sands suggests a transgressive marine deposition with wave-induced densification; at a 'screening level', the Merritt Sand exhibits $-0.10 > \psi > -0.20$, although this range reflects systematic change across the site with CPT-2018-11A encountering looser conditions ($\psi_k \sim -0.12$) than CPT-2018-10A ($\psi_k \sim -0.17$) throughout the Merritt and with the third CPT-2018-09A lying in the middle.

As previously discussed, there are multiple sub-units within the underlying Pleistocene Bay Mud. Layer 7 presents as over-consolidated and/or dense to the extent of being quite dilatant; the undrained strength ratios commonly exceed $s_u/\sigma'_{v0} > 0.7$ using $N_{kt} = 16$. Layer 8, despite being identified as a separate layer on the depth record, is present in the same place in terms of soil behavior type. Layer 9, despite underlying 7, appears as slightly more plastic but certainly less over-consolidated; this could reflect a lower friction angle and/or greater compressibility rather than the geologically difficult less over-consolidation per se. Undrained strength ratios are largely in the range $0.4 < s_u/\sigma'_{v0} < 0.6$ using $N_{kt} = 16$.

## 6. Ground motion during event

The October 17, 1989 Loma Prieta earthquake had a magnitude of 6.9, with an epicenter at approximately 16 km northeast of Santa Cruz. The effects of the Loma Prieta earthquake extended well to the north into the San Francisco Bay area, including Alameda (at an epicentral distance of some 85 km). The recorded ground motion at the Yerba Buena Island (YBI; $V_{S30} = 660 m/s$, where $V_{S30}$ is the time-averaged shear-wave velocity in the top 30 m) has been used as that of bedrock for studies at Alameda, including the HBBP. The nearest site to HBBP
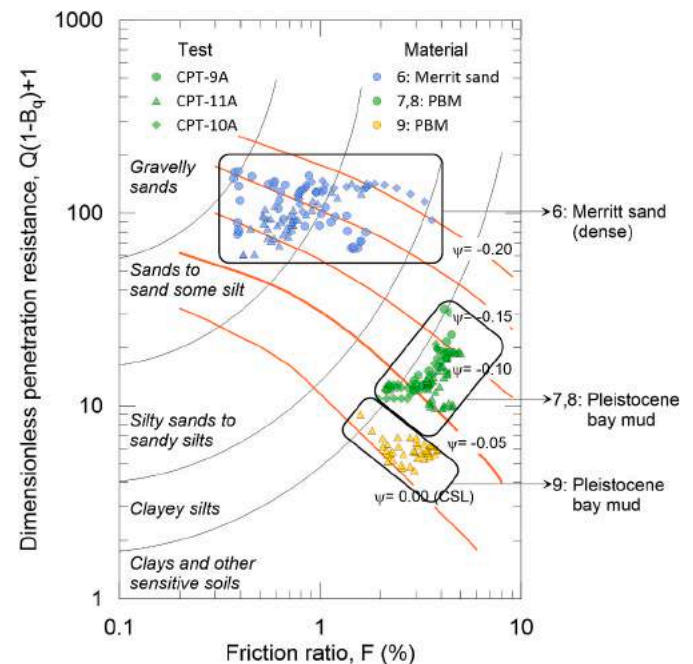


**Fig. 20.** Computed undrained triaxial compression of Bay Mud using Norsand calibrated properties.



**Fig. 21.** CPT data within the Pleistocene sediments, plotted by soil behavior type.

with a recording strong-motion station at the time was the Naval Air Station (NAS; $V_{S30} \approx 150 \, m/s$), about 7 km distant, and the outcrop motion at YBI correlates with that of the surface at the NAS with an approximate time delay of 320 ms, illustrated in Fig. 22. Of note, the same stratigraphic sequence is found at HBBP and NAS; in addition, the $V_{S30}$ are similar for the two sites, thus we will use it as the surface ground motion. The motion of the NAS site stays aligned with that of the bedrock until approximately 12 seconds elapsed time (taking the origin of the NAS record as the start of the recording). At that instant, the NAS site can no longer follow the motion of the bedrock and the two motions decouple. It is inferred this decoupling is caused by liquefaction or similar of the upper loose soils at 12 seconds, with the upper part of the site (including the hangar with the strong motion station) then "wobbling" on the softened/liquefied ground largely independent of basal acceleration. The ratio of accelerations at the top and bottom parts of the soil profile is approximately constant (a factor of 3.75) during the time interval 0–12 seconds of the two records, as observed in Fig. 22, where the 3.75 factor is already applied. The decoupling can also be observed by assessing the change in the frequency content of the ground motion through the use of a Stockwell transform (Stockwell et al. [39]), which depicts the time-frequency distribution of a ground motion recording. Fig. 23 shows the Stockwell transforms for the NAS and Yerba Buena records; it can be observed that the large frequencies (i.e., larger than 5hz) in the Yerba Buena record are not present in the NAS record after approximately 12 s when the most intense part of the ground motion occurs which may have caused increased excess pore pressures and a loss in stiffness, which in turn shifts the motion to higher periods (lower frequencies). Similar observations were made for ground motions recorded at liquefied sites by Kramer et al. [40] and Macedo and Bray [41].

We also focus on the ground motion between recorded times of 8 s–16 s, which is the portion of the record where the strongest motion occurred. We estimated that there are about 5 'significant' cycles within this portion of the record which were subsequently followed by much-reduced amplitude motions for a further 10 seconds or so. The number of 'significant' loading cycles is about half what would usually be associated with an earthquake of Loma Prieta's magnitude, and it may be related to the particularities associated with the fault rupture in the Loma Prieta earthquake.

## 7. Liquefaction observations

### 7.1. Manifestation of liquefaction

Liquefaction at the HBBP was manifested as sand boils south of Harbor Bay Parkway, in the ITP, west of South Loop Road in the Airport
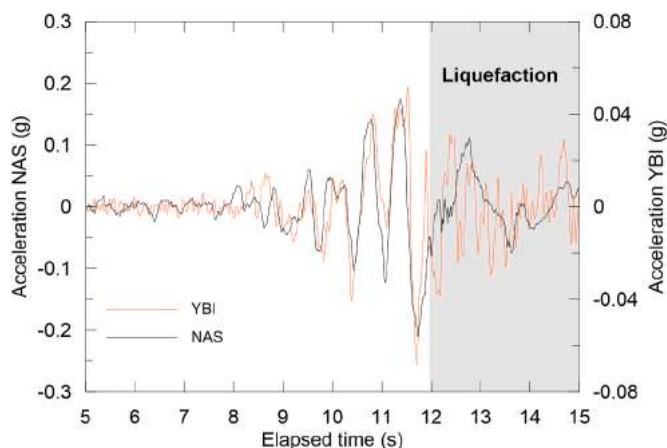


**Fig. 22.** Comparison of ground motions at the NAS recording station with the bedrock ground motion recorded at the YBI station.

Center and surgical dynamics sites, and along the north side of Harbor Bay Parkway north and west of the ITP. Sand boils were apparent around the ITP buildings and in the undeveloped areas throughout the 0.12 km$^2$ ITP site, see Fig. 1. There were several locations in the HBBP where thin cracks were apparent in the ground surface. Some of these cracks extended for substantial distances and were side by side and acted as conduits for the upward movement of sand and water that emerged as sand boils. Other man-made conduits, such as the location of manholes, drop inlets, and risers for pipes, provided similar conduits. Typically, the pressurized sand and water flowed up along the side of these structures to the ground surface and migrated out onto the ground surface; Fig. 24 below illustrates this aspect.

Two identical two-story concrete-framed office buildings had been built within the ITP before 1989. It was recognized that the loose fill sands could liquefy, and the buildings were designed with this in mind. The two structures were supported on spread footings bearing in the ubiquitous dense sand that caps the site, with footing elevations providing a distance of at least twice footing width to the base of the dense sand. Numerous sand boils were apparent around the ITP buildings after the earthquake. Ejected sand emerged through a saw cut made through the ground floor slab in one building a few days before the earthquake, filling the room with a few inches of sand. Earthquake-induced settlements (estimated from notes made at the time) were in the order of 100–150 mm, some of which may have been caused by "loss of ground" associated with the development of sand boils at the ITP.

## 8. Site liquefiability

### 8.1. Cyclic stress ratios

The shear stresses at a given depth were estimated as $\tau = \frac{a}{g}\sigma_v r_d$ where $a$ is the acceleration time history at the surface, $\sigma_v$ is the total stress at a given depth, and $r_d$ is a depth-dependent factor that modifies the $a$ to account for the flexibility in the dynamic response of a soil mass. We used the $r_d$ factors from Boulanger and Idriss [42]. The estimated $\tau$ time-history at the middle of layer 5 (~7.5 m depth) is presented in Fig. 25. The cyclic stress ratio (CSR) at a given depth was estimated as $CSR = 0.65 \frac{\tau_{max}}{\sigma_v'}$, where $\sigma_v'$ is the effective vertical stress at a given depth. For example, CSR for layer 2 varies from 0.10 to 0.15.

### 8.2. Holocene Bay Mud

The cyclic strength of the Bay Mud at five cycles, which is the estimated number of significant cycles in the Loma Prieta record, derives on a cyclic resistance ratio (CRR) of about 0.25 (Fig. 10). This is less than the peak demand apparent in Fig. 25. Focusing on strength misses an important aspect of Bay Mud behavior. Referring to Fig. 20, the Bay Mud's stress-strain behavior, regardless of $\psi$, is near bi-linear with a relatively stiff initial response followed by an important loss of stiffness once the mobilized strength ratio $s_y/\sigma_{v0}' > 0.2$ (and possibly as little as 0.16) where we are now associating the loss of stiffness as a "yield" condition. The strength-demand represented by the CSR time history shown in Fig. 25 could not be transmitted by the Bay Mud beyond the second-pulse at about 11 s elapsed time when $\tau > s_y$, which is exactly the behavior seen in the strong-motion record at the geologically similar NAS site and at near-enough the same point in the record (see Fig. 22 at 12 seconds). It is not that the Bay Mud is 'liquefiable' but rather that Bay Mud is simply a weak clayey silty material with an abrupt yield into a near fully-plastic deformation; hence, limiting the stresses transmitted to the overlying sands (see discussion section).

### 8.3. Sand fill

Liquefaction assessment charts/procedures, and strength trends, are normalized to 15 loading cycles. As there were approximately 5 cycles in
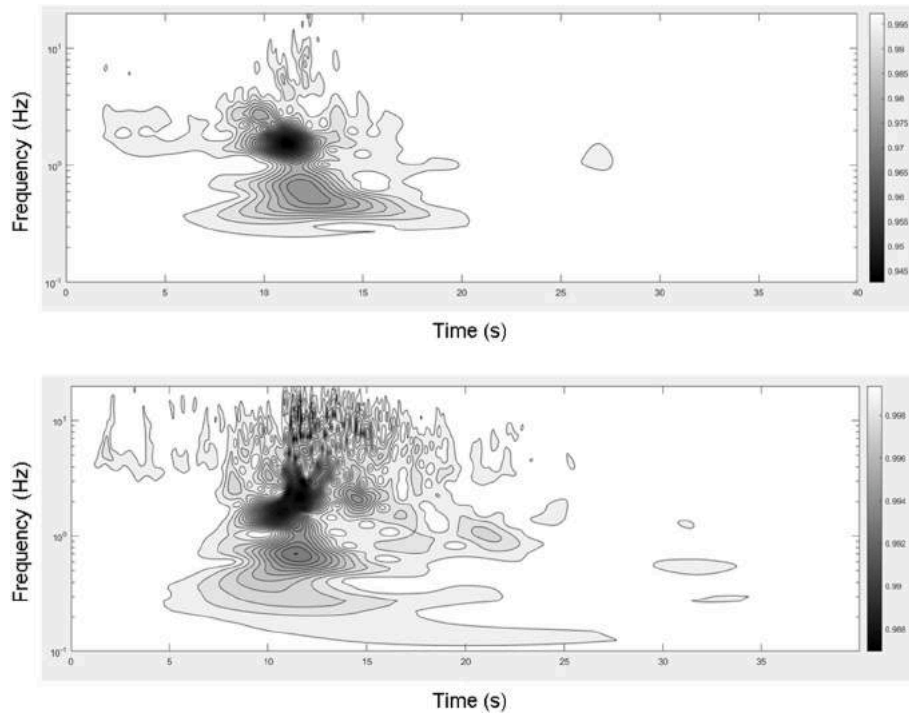
**Fig. 23.** Top: Stockwell transform of the acceleration-time history recorded at the top of the NAS station. Bottom: Stockwell transform of the acceleration-time history recorded at the Yerba Buena station.



**Fig. 24.** Example of liquefied sand transported to the surface of the building periphery (1320 Harbor Bay Parkway).



**Fig. 25.** Estimated cyclic stress ratio history at the middle of Layer 5.

the Loma Prieta record, the sand fill at the ITP will behave 'stronger' because of the reduced demand on it. Laboratory data suggest that a 15-to-5 cycle scaling would amount to an apparent strength increase by a factor of approximately 1.3–1.4 (Jefferies and Been [43]).

The in-situ state parameter of the majority of the loose fill, Layer 2 of the site characterization (Fig. 3), shows natural variability. Stochastic simulations (Popescu et al. [44–47]) indicate that about the loosest 20% of a formation controls its behavior, commonly referred to as the characteristic value from the distribution (and denoted by the subscript 'k'). A reasonable judgement is that layer 2 has -0.02 < $\psi_k$ < 0.10.

The assessed demand and in-situ states are shown on a liquefaction triggering chart, Fig. 26. This chart uses the "Class A" case-histories of Moss [48], updated to a characteristic state parameter (Jefferies and Been [43]), which is only valid for $F < 1.3$. Most, but not all, of the data for Layer 2 fall within this friction ratio limit of validity (Fig. 12). The loose hydraulic fill, despite the potential role of the Bay Mud on limiting
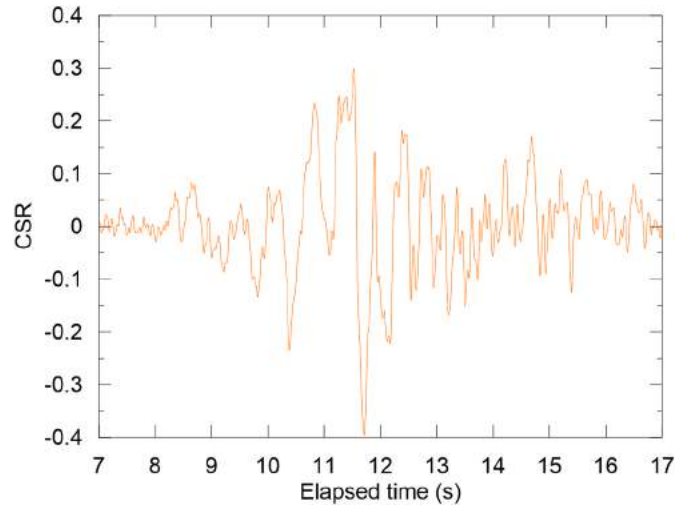
the transmitted shear stresses, presents as liquefiable.

### 8.4. Merritt Sand

In terms of the liquefaction response of the Merritt sand during the Loma Prieta earthquake, a comparison of the assessed characteristic state of the Merritt sand ($-0.12 > \psi_k > -0.17$) discussed earlier with the liquefaction triggering criteria shown in Fig. 26, derives in a CRR of about 0.25, which when compared against the estimated CSR at the top of the Merritt sand, which is in the order of 0.16 using the procedures in the "cyclic stress ratio" section (after a correction for the number of cycles as discussed in section 8.1), shows the Merritt sand as not liquefiable. A further factor is that the Merritt sand presents on the soil behavior type chart (Fig. 21) as relative compressible, a factor that will also attenuate induced excess pore pressures during cyclic loading. Thus,
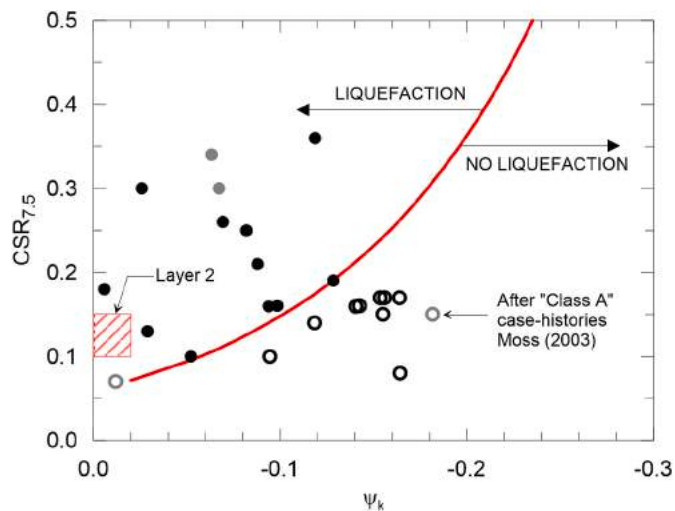
**Fig. 26.** Comparison of assessed in-situ state with vulnerability to earthquake-induced liquefaction. Note that the x-axis is inverted to highlight negative state parameters.

it is reasonable to treat the Merritt sand as having maintained its shear stiffness during the Loma Prieta earthquake.

### 9. Discussion

The classification of fine-grained soils as "clay-like" is purely geological and neglects their intrinsic behavior. On a geological classification, the Bay Mud would be "clay-like" as per Idriss and Boulanger [49] (the plasticity index is significantly higher than 7) and treated for liquefaction purposes accordingly. A feature of "clay-like" is that only stress-history is important; however, the Bay Mud shows a spectrum of void ratios with no normal compression zone apparent when plotting in-situ void ratio versus effective stress of the sample (Fig. 8). In fact, regarding the field void ratios measured in the Bay Mud, if the y-axis scale were hidden from the viewer, the range of void ratios would look as "sand-like." This is not a limitation for the selected approach in this study as critical state theory does not allow separation into "sand-like" or "clay-like" behavior, with the same equations applying across the spectrum from soft clay through to (at least) coarse sand – it is just a question of the numerical values for the soil properties. Interestingly, the application of the critical state theory to Bay Mud gives a consistent fit of the computed state and the corresponding undrained strength to independent measurements. This, in turn, then shows that Bay Mud is a weak soil with full-plastic yielding at about half the demand of the Loma Prieta earthquake. Thus, focusing on a critical layer within the sand simply misses the importance of the Bay Mud and its interaction with the fill units. In this regard, looking to the full profile of the soil on the CPT leads to the same conclusions as Cubrinovski [50]: site details matter.

In terms of the interaction between the Bay Mud and the fill layers, strictly speaking, the monotonic response of the Bay Mud (presented in Fig. 20) does not answer the issue of unloading between cycles; however, theory suggests that unloading-reloading is stiff even when the original loading may have reduced the soil's strength significantly. Moreover, our computed stress-strain behavior allowing for the looser in-situ states does not predict strain-softening (see Fig. 20). Thus, this suggests that the role of the Bay Mud is limiting the transmitted shear stresses rather than acting as a true filter of high-frequency motion. Hence, it is reasonable to expect that much of the filtering may have occurred on the liquefied fill, with some contribution from the Bay Mud, especially during the strong part of the shaking. This compounded behavior for the Bay Mud and the loose fill is consistent with the sudden decoupling of bedrock and site motions at the geologically similar Naval Air Station. Finally, despite the potential role of the Bay Mud in limiting

the transmitted stresses, the evidence of sand boils (Fig. 24) suggests that this was not sufficient to protect the hydraulic sand fill: there was sand liquefaction at the ITP. This should not come as a surprise as, even after scaling for the short duration of the Loma Prieta event, the in-situ state of the fill sands was such that the onset of earthquake-induced liquefaction was to be expected.

### 10. Conclusion

The vulnerability of the International Telegraph Plaza (ITP) to earthquake-induced liquefaction has been assessed using a critical state approach; this approach explicitly includes soil properties as opposed to only fine contents corrections, which are not fundamentally anchored on mechanics in our view. A consistent pattern of the various measurements is revealed, with the inferred state of the hydraulic fill and the soft underlying Bay Mud, leading to an expected performance in the Loma Prieta earthquake that matches that encountered. Interesting aspects of this approach were the ease with which actual soil properties were included and the further ease of dealing with the wide range of soil gradations within the fill.

### Author statement

**Jorge Macedo:** Conceptualization, Writing- Original draft, Methodology, Investigation, Supervision, Funding acquisition. **Luis Vergaray:** Data curation, investigation, Writing- Original draft. **Curtis Jensen:** Visualization, Investigation, Resources. **Renzo Cornejo:** Visualization, Writing- Original draft. **Michael Jefferies:** Conceptualization, Writing- Original draft, Data Curation.

### Declaration of competing interest

The authors declare that they have no known competing financial interests or personal relationships that could have appeared to influence the work reported in this paper.

### Acknowledgment

### References

[1] Mitchell JK, Lodge AL, Coutinho RQ, Kayen RE, Seed RB, Nishio S, Stokoe KH. In situ test results from four Loma Prieta earthquake liquefaction sites: SPT, CPT, DMT and Shear Wave Velocity: Berkeley. Report UCB/EERC-94/04. University of California Earthquake Engineering Research Center; 1994. p. 179.

[2] Moss RE, Seed RB, Kayen RE, Stewart JP, Der Kiureghian A, Cetin KO. CPT-based probabilistic and deterministic assessment of in situ seismic soil liquefaction potential. J Geotech Geoenviron Eng 2006;132(8):1032–51.

[3] Hallenbeck, Associates. Response of ground to Santa Cruz earthquake (sic) of October 17, 1989. Letter to Doric Development; October 20, 1989.

[4] Youd TL, Idriss IM, Andrus RD, Arango I, Castro G, Christian JT, Dobry R, Liam Finn WD, Harder Jr LF, Hynes ME, Ishihara K, Koester JP, Liao SSC, Marcuson III WF, Martin GF, Mitchell JK, Moriwaki Y, Power MS, Robertson PK, Seed RB, Stokoe II KB. Liquefaction resistance of soils: summary report from the 1996 NCEER and 1998 NCEER/NSF workshops on evaluation of liquefaction resistance of soils (NCR method). J Geotech Geoenviron Eng 2001;127:10. https://doi.org/10.1061/(ASCE)1090-0241(2001)127:10(817).

[5] Lyman. Construction of Franklin falls dam. Report, US Army Corps of Engineers. 1938.

[6] Casagrande A. Characteristics of cohesionless soils affecting the stability of slopes and earth fills. Harvard University; 1936.

[7] Casagrande A. Liquefaction and cyclic deformation of sands, a critical review. Buenos Aires: Proceedings of 5th Pan American Conference Soil Mechanic, Foundation Engineering; 1975. p. 80–133.

[8] Taylor DW. Fundamentals of soil mechanics. New York: John Wiley; 1948.

[9] Bishop AW. Reply to discussion on "Measurement of shear strength of soils" by A. W. Skempton and A.W. Bishop. Géotechnique 1950;2:90–108.

[10] Been K, Jefferies MG. A state parameter for sands. Geotechnique 1985;35(2): 99–112.

[11] Jefferies MG. On the fundamental nature of the state parameter. Géotechnique 2021. https://doi.org/10.1680/jgeot.20.P.228.

[12] Morgenstern N, Vick S, Viotti C, Watts B. Fundão tailings dam review panel report on the immediate causes of the failure of the Fundão dam. Samarco S.A., Vale S.A; 2016.

[13] Morgenstern NR, Jefferies M, Zyl DV, Wates J. Independent technical review board. Report on NTSF embankment failure. Ashurst Australia; 2019. Available at: https://www.newcrest.com/sites/ default/files/2019-10/190417_Report%20on% 20NTSF%20Embankment%20Failure%20at%20Cadia %20for%20Ashurst.pdf.

[14] Robertson PK, De Melo L, Williams DJ, Wilson GW. Report of the expert panel on the technical causes of the failure of Feijão dam I. 2019. Available at: http://www. b1technicalinvestigation.com/.

[15] Arroyo M, Gens A. Computational analyses of dam I failure at the Corrego de Feijao mine in Brumadinho – final report. Vale S.A; 2021.

[16] Stamatopoulos CA. An experimental study of the liquefaction strength of silty sands in terms of the state parameter. Soil Dynam Earthq Eng 2010;30(8):662–78.

[17] López-Querol S, Coop MR. Drained cyclic behaviour of loose Dogs Bay sand. Geotechnique 2012;62(4):281–9.

[18] Qadimi A, Mohammadi A. Evaluation of state indices in predicting the cyclic and monotonic strength of sands with different fines contents. Soil Dynam Earthq Eng 2014;66:443–58.

[19] Pan K, Yang ZX. Effects of initial static shear on cyclic resistance and pore pressure generation of saturated sand. Acta Geotechn 2018;13(2):473–87.

[20] Wei X, Yang J. Cyclic behavior and liquefaction resistance of silty sands with presence of initial static shear stress. Soil Dynam Earthq Eng 2019;122:274–89.

[21] Rogers JD, Figuers SH. Engineering geologic site characterization of the greater Oakland Alameda area, Alameda and san Francisco Counties, California. Report to the National Science Foundation, report number: Grant No. BCS 9003785. 1992. https://doi.org/10.13140/RG.2.1.4785.6809.

[22] Langan Engineering and Environmental Services, Inc. Geotechnical investigation Harbor Bay South Loop. Report to srmErnst Development Partners. Alameda California; 29 March 2019.

[23] USGS. U.S. Geological Survey. 1992. https://pubs.er.usgs.gov/publication /70043734.

[24] Jefferies M, Been K. Soil variability and characteristic states. Soil liquefaction: a critical state approach. CRC Press; 2016. p. 203–24.

[25] Jefferies MG, Been K. Soil liquefaction – a critical state approach. London and New York: Taylor & Francis Group; 2006, ISBN 0-419-16170-8.

[26] Sitar N, Salgado R. Behavior of the san Francisco Bay Mud from the Marina district in static and cyclic simple shear. Geotechnical Engineering Report No. UCB/GT/ 93-03. Berkeley, CA: Department of Civil Engineering, University of California; April 1993. p. 20.

[27] Rau GA, Sitar N. Post-cyclic response of Holocene Bay Mud from san Francisco. Geotechn Earthq Eng Soil Dynam 1998;III:246–57.

[28] Parks MC. Engineering properties and geologic setting of old Bay clay deposits. Downtown San Francisco, California: UC Berkeley; 2019. ProQuest ID: Parks_ berkeley_0028E_19138. Merrit ID: ark:/13030/m5jx3mp6. Retrieved from, htt ps://escholarship.org/uc/item/7zx826gw.

[29] Meehan CL, Duncan JM, Brandon TL, Boulanger RW. An experimental study of the dynamic behavior of slickensided surfaces. Report of a study performed by the Virginia. Tech Center for Geotechnical Practice and Research; 2006.

[30] Campanella RG, Robertson PK, Gillespie D. Seismic cone penetration test. Use of in-situ tests in geotechnical engineering (GSP 6). Reston/VA: ASCE; 1986. p. 116–30.

[31] Shuttle D, Jefferies M. Determining silt state from CPTu. Geotechn Res 2016;3(3): 90–118. https://doi.org/10.1680/jgere.16.00008. Available at:.

[32] Plewes HD, Davies MP, Jefferies MG. CPT based screening procedure for evaluating liquefaction susceptibility. In: Proceedings of the 45th Canadian geotechnical Conference; 1992. Canada, Toronto.

[33] Reid D. Estimating slope of critical state line from cone penetration test—an update. Can Geotech J 2015;52(1):46–57. https://doi.org/10.1139/cgj-2014-0068.

[34] Been K, Jefferies MG. Towards systematic CPT interpretation. In: Proceedings of the Wroth memorial symposium. London: Thomas Telford; 1992. p. 121–34.

[35] Mitchell JK, Wentz Jr FJ. Performance of improved ground during the loma Prieta earthquake. University of California Berkeley, Earthquake Engineering Research Center; 1992. Report No. UCB/EERC-91/12.

[36] Reid D, Jefferies M. State parameter as a geological principle in tailings. In: Wilson G Ward, Sego DC, Beier NA, editors. Proceedings of tailings and mine waste 2017. Edmonton: University of Alberta Geotechnical Center; 2017. p. 305–14.

[37] Jefferies MG. Nor-Sand: a simple critical state model for sand. Geotechnique 1993; 43(1):91–103.

[38] Ghafghazi M, Shuttle D. Interpretation of sand state from cone penetration resistance. Geotechnique 2008;58(8):623–34. https://doi.org/10.1680/ geot.2008.58.8.623.

[39] Stockwell R, Mansinha L, Lowe RP. Localization of the complex spectrum: the S transform. IEEE Trans Signal Process 1996;44(4):998–1001. https://doi.org/ 10.1109/78.492555.

[40] Kramer S, Sideras S, Greenfield M. The timing of liquefaction and its utility in liquefaction hazard evaluation. Soil Dynam Earthq Eng 2016;91:133–46. https:// doi.org/10.1016/j.soildyn.2016.07.025.

[41] Macedo J, Bray J. Key trends in assessment of Liquefaction-Induced building settlement from numerical analyses. Am Soc Civ Eng (ASCE/JGGE) J 2018;144 (11). https://doi.org/10.1201/(ASCE)GT.1943-5606.0001951.

[42] Boulanger R, Idriss IM. CPT-Based liquefaction triggering procedure. J Geotech Geoenviron Eng 2016;142(2).

[43] Jefferies MG, Been K. Soil liquefaction: a critical state approach. second ed. Boca Raton, FL, USA: CRC Press; 2015. https://doi.org/10.1680/b19114. Available at:.

[44] Popescu R, Prevost JH, Deodatis G. Effects of spatial variability on soil liquefaction: some design recommendations. Geotechnique 1997;475:1019–36.

[45] Popescu R, Prevost JH, Deodatis G. Spatial variability of soil properties: two case studies. Geotechnical earthquake engineering and soil dynamics. Geotechnical Special Publication No. 75. Seattle: ASCE; 1998. p. 568–79.

[46] Popescu R, Deodatis G, Prevost JH. Simulation of non-Gaussian homogeneous stochastic vector fields. Probabilist Eng Mech 1998;13(1):1–13.

[47] Popescu R, Prevost JH, Deodatis G. Characteristic percentile of soil strength for dynamic analyses. Geotechnical Earthquake Engineering and Soil Dynamics. Geotechnical Special Publication No. 75. ASCE; 1988. p. 1461–71.

[48] Moss RES. CPT-based probabilistic assessment of seismic soil liquefaction initiation. Ph.D. dissertation. University of California Berkeley; 2003.

[49] Idriss IM, Boulanger RW. Soil liquefaction during earthquake. Oakland, California, USA: EERI publication, Monograph MNO-12, Earthquake Engineering Research Institute; 2008.

[50] Cubrinovski M. Some important considerations in the engineering assessment of soil liquefaction. In: Acosta-Martinez H, Lehane BM, editors. Proc., 13th Australia New Zealand Conf. on geomechanics; 2019. p. 19–36.